PCCP

Accepted Manuscript

ROYAL SOCIETY OF CHEMISTRY

www.rsc.org/pccp

Journal Name

RSCPublishing

COMMUNICATION

Tavorite-$FeSO_4F$ as a potential cathode material for Mg ion batteries: a first principles calculation

Cite this: DOI: 10.1039/xoxxoooooox

Jiandong Wu, Guohua Gao*, Guangming Wu*, Bo Liu, Huiyu Yang, Xiaowei Zhou, Jichao Wang

Received ooth January 2012,
Accepted ooth January 2012

DOI: 10.1039/xoxxoooooox

www.rsc.org/

The electrochemical and Mg ion diffusion properties of tavorite-$Mg_{0.5}FeSO_4F$ was studied by using First principles calculations. A discharge voltage about 2.52 V versus Mg/Mg^{2+} corresponding to the redox couples of Fe^{3+}/Fe^{2+} was predicted for tavorite-$Mg_{0.5}FeSO_4F$, and the experimental diffusion coefficient for Mg-vacancy in $Mg_{0.5-x}FeSO_4F$ is expected to be in the same order of magnitude with that of Li-vacancy in $Li_{1-x}FeSO_4F$.

Rechargeable batteries with high specific energy, high safety and high specific power density are critical for clean and recyclable energy storage. Li ion batteries, Li-air battery and Li-Sulfur battery have been widely studied. Especially, lithium ion batteries (LIBs) have already been used in portable electronic devices. Besides, Mg ion batteries (MIBs) were also studied because of its safety of handling, higher volumetric energy density and low cost. Since Aurbach et al. assembled a prototype rechargeable magnesium batteries[1] in standard coin cells, many researchers have been working toward developing new cathode materials for MIBs. Tao et al. studied the electrochemical properties of TiS_2 nanotubes[2] as a cathode material for Mg ion batteries, and a discharge capacity about 236 $mAhg^{-1}$ was achieved at 10 mAg^{-1}. Ichitsubo et al. found that magnesium complex oxides[3] such as $MgCo_2O_4$, $Mg_{0.67}Ni_{1.33}O_2$ and $MgNiO_2$ exhibit high open circuit voltage exceeding 3V. Mitelman et al. found that $CuMo_6S_8$ can serve as a fast cathode material for rechargeable Mg ion batteries[4]. Liang et al. assembled a battery with graphene-like MoS_2 cathode and ultrasmall Mg particles[5], which exhibits a voltage of 1.8 V and a reversible capacity about 170 $mAhg^{-1}$. Although much significant research about Mg ion batteries has been performed, only a few materials can serve as cathode for MIBs. One of the obstacles is the low Mg ions mobility in most of the cathode materials[6-8]. Hence, develop new cathode materials with high Mg ion mobility is critical for the development of MIBs. It is worth noting that first principles calculations has been widely used to predict the diffusion coefficients for Li^+ and Mg^{2+} in electrode materials[9-18]. By performing first principles calculations, many host materials such as V_2O_5[15], Zigzag MoS_2 Nanoribbon[12], $MgFeSiO_4$[19], $CaFe_2O_4$-type $MgMn_2O_4$[20] and $MgVPO_4F$[14] have been investigated as electrode materials in MIBs. By far as we know, the theoretical study of $FeSO_4F$ as a cathode materials for MIBs has not been performed.

It is known that $LiFeSO_4F$ exist in two polymorphs[21]: tavorite and triplite. In addition, theoretical study expected that the tavorite form would have batter Li^+ transport property than triplite form[22]. In this paper, the crystal structures of tavorite-$FeSO_4F$ and $Mg_{0.5}FeSO_4F$ were studied by performing first principles calculations. The OCV for $Mg_{0.5}FeSO_4F$ as cathode materials for MIBs were predicted, and the electronic structures and Bader charge for Mg_xFeSO_4F(x=0, 0.5) were studied in detail to reveal the redox mechanism as Mg insert into tavorite-$FeSO_4F$. Finally, the energy barrier for Mg-vacancy diffusion along [010] direction of the super cell was investigated.

All the calculations in this paper were performed using the Vienna ab initio simulation package (VASP)[23], the exchange and correlation energy functional was treated by the Perdew–Burke–Ernzerh of variant of the generalized gradient approximation (GGA)[24]. GGA+U[25] approach was used to take into account the strongly correlated character of the d electrons of Fe atoms, and the U_{eff}=4.0 eV was adapted for Fe, similar values have been used in Ref[26] and Ref[21]. Interaction between ion and electrons were described with projector augmented wave pseudo potentials (PAW)[27, 28] approach. The following electronic states were treated as valance electrons: $Fe(3d^74s^1)$, $S(3s^23p^4)$, $O(2s^22p^4)$, $F(2s^22p^5)$, $Li(2s^12p^0)$, and the cut off energy for the plane wave basis set was set to be 500 eV, and the total energy was converged to 10^{-5} eV. In addition, the spin polarization was taken into account along with the ferromagnetic (FM) and antiferromagnetic (AFM) arrangement. A k-points sampling of 5×5×5 was used to ensure the energies were converged within 5 meV per formula unit. To investigate Mg ion diffusion kinetics, a super cell containing 1×2×1 unit cells was constructed, and k-points sampling of 3×1×3 was used. The activation barriers

were calculated with the climbing-image nudged elastic band (Cl-NEB)[29] method implemented in VASP, and the Cl-NEB calculations were deemed to be converged when the force on each image was less than 0.03 eVÅ^{-1}.

The crystal structure of tavorite-$LiVPO_4F$ was used as a template and a super cell containing four formula units of tavorite-$LiFeSO_4F$ was constructed. To obtain the crystal structure of $Mg_{0.5}FeSO_4F$, two of the four Li ions were replaced with Mg ions, and the other two Li ions were removed. The most stable Mg ions configurations for $Mg_{0.5}FeSO_4F$ were used for the following calculations. To obtain the crystal structure of $Mg_{0.25}FeSO_4F$ and $FeSO_4F$, Mg ions were removed from $Mg_{0.5}FeSO_4F$ and following with fully relaxation. The calculations predict an AFM ground states for both $Mg_{0.5}FeSO_4F$ and $FeSO_4F$. The stability of intermediate phase $Mg_{0.25}FeSO_4F$ was analysed by calculating the formation energy of $Mg_{0.25}FeSO_4F$ with the following expression:

$$E_f = E(\mathrm{Mg}_{0.25}\,FeSO_4F) - [0.5E(\mathrm{Mg}_{0.5}\,FeSO_4F) + 0.5E(FeSO_4F)]$$

Where $E(Mg_xFeSO_4F)$ is the total energy per formula of Mg_xFeSO_4F. The formation energy for the most stable configuration of $Mg_{0.25}FeSO_4F$ is 0.05 eV per formula, indicating that solid solution $Mg_{0.25}FeSO_4F$ is energetically unfavorable at low temperature. Hence, phase separation of $Mg_{0.5}FeSO_4F/FeSO_4F$ is expected when Mg is extracted from $Mg_{0.5}FeSO_4F$ and a flat charge/discharge voltage curve was predicted for $Mg_{0.5}FeSO_4F/FeSO_4F$.

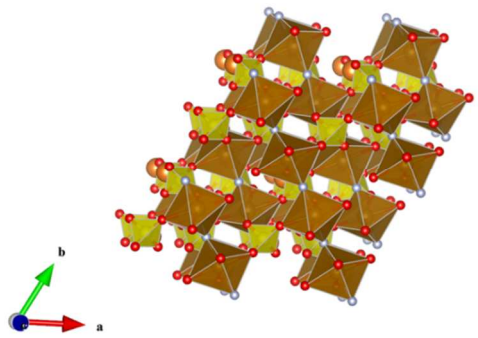

Fig.1 Crystal structure of $Mg_{0.5}FeSO_4F$: the golden yellow octahedra represent FeO_4F_2, the yellow tetrahedron represent SO_4, the red spheres represent O, the dark gray spheres represent F and the orange spheres represent Mg.

The crystal structure of $Mg_{0.5}FeSO_4F$ was shown in Fig.1. Fe atoms locates in an octahedral site, FeO_4F_2 octahedra connect each other through F atoms, forming a 1-D chain along [-110] direction. The SO_4 tetrahedra share corners with FeO_4F_2 octahedra and link the FeO_4F_2 octahedra together.

Table 1 The lattice parameters of $FeSO_4F$ and $Mg_{0.5}FeSO_4F$.

		a(Å)	*b*(Å)	*c*(Å)	*α*(°)	*β*(°)	*γ*(°)	*V*(Å^3)
$FeSO_4F$	This work (unit cell)	7.026	7.400	7.720	91.215	90.274	61.231	351.726
	This work (primitive cell)	5.207	5.232	7.354	107.695	109.285	95.394	175.865
	Calc.[21]	5.226	5.216	7.388	108.397	109.783	93.708	176.464
	Exp.[30]	5.074	5.082	7.336	110.975	111.189	88.157	163.640
$Mg_{0.5}FeSO_4F$	This work (unit cell)	7.199	7.764	8.048	91.312	92.069	60.554	391.508
	This work (primitive cell)	7.199	7.560	8.048	89.378	87.931	63.424	391.508

The obtained lattice parameters of tavorite-$FeSO_4F$ and $Mg_{0.5}FeSO_4F$ are compared with previous theoretical and experimental data as shown in Table1. $FeSO_4F$ is crystallized in the triclinic space group P-1 with two iron atoms occupy at 1a (0, 0, 0) and 1b (0, 0, 1/2) site respectively, and with O, S and F atoms occupy at 2i sites. The lattice parameters for primitive cell are in good agreement with previous calculation[21]. The computed volume is about 7.4% larger than the experimental value[30], and the lattice parameters are slightly overestimated compared with the experimental values[30], which is a reasonable error for the use of GGA+U[17, 31]. $Mg_{0.5}FeSO_4F$ is also crystallized in the triclinic space group P-1 but with all the atoms occupy at 2i sites, and only the cell shape were changed after impose symmetry on the unit cell. The volume expansion from $FeSO_4F$ to $Mg_{0.5}FeSO_4F$ is about 11%, which is similar with the volume change as the lithiation of $FeSO_4F$.

The average OCV was obtained by calculating the difference of Mg chemical potential between cathode (tavorite-$FeSO_4F$) and anode (Mg).[20]

$$E_{OCV} = \frac{E_{tot}(Mg_{x2}TMPO_4F) - E_{tot}(Mg_{x1}TMPO_4F) + (x2 - x1)E_{tot}(Mg)}{(x2 - x1)Fz}$$

Where $E_{tot}(Mg_{x1}FeSO_4F)$ and $E_{tot}(Mg_{x2}FeSO_4F)$ are the total energy of $Mg_{x1}FeSO_4F$ and $Mg_{x2}FeSO_4F$ respectively, $E_{tot}(Mg)$ represents the energy of metallic Mg in hexagonal structure. Moreover, F is the Faraday constant and z is the charge (electrons carried by Mg^{2+}). The chemical potential of the Mg metal with a hexagonal structure was considered as the anode material, and a Monkhorst-Pack mesh of (15×15×15) of k-points was used for calculations of metallic Mg.

The calculated OCV for Mg extraction from $Mg_{0.5}FeSO_4F$ is about 2.52 V versus Mg/Mg^{2+}. The voltage for magnesiation was about 1.1 V lower than that of lithiation (3.62 V[26]), which is similar with the voltage for magnesiation and lithiation of olivine compounds[19].

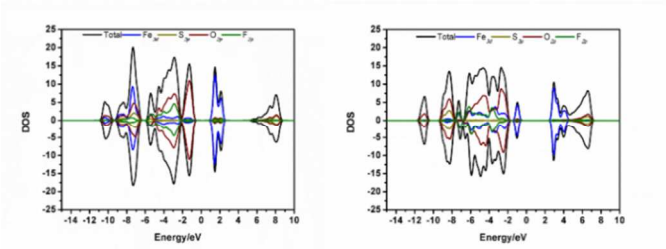

Fig.2 DOS and PDOS for (a) $FeSO_4F$ and (b) $Mg_{0.5}FeSO_4F$. The Fermi level is set at zero energy.

In order to analyse the reduction mechanism as Mg insert into $FeSO_4F$, the total density of states (TDOS) and partial density of states (PDOS) of $FeSO_4F$ and $Mg_{0.5}FeSO_4F$ with AFM order were calculated. For $FeSO_4F$, the states of O_{2p} between -9 eV and -5 eV are overlap strongly with S_{3p} states. This indicated the existent of S_{3p}-O_{2p} covalent bond in $FeSO_4F$. The strong overlap between Fe_{3d} and O_{2p} (F_{2p}) states is obvious, indicating that the covalent Fe-O(F) bond is formed between Fe_{3d} and O_{2p} (F_{2p}) states. The valance states near the Fermi level are dominated by O_{2p} orbital, and the states at bottom of conduction band are mainly contributed by Fe-3d orbitals, indicating that $FeSO_4F$ appears to be a charge-transfer (CT) insulator. As Mg insert into $FeSO_4F$ to form $Mg_{0.5}FeSO_4F$, the Fermi level shift toward higher energy. The results also confirm the covalent bond between S_{3p} and O_{2p} and between Fe_{3d} and O_{2p} (F_{2p}) states, which indicating the crystal structure was stable after the Mg ions intercalation. And an additional Fe_{3d} band is filled, which is known as the lower Hubbard bands. The Fe_{3d} band in the conduction band are found between 2.5 eV and 4.5 eV, which form the upper Hubbard bands. These features show that $Mg_{0.5}FeSO_4F$ is most likely a Mott-Hubbard (MH) insulator. Hence, a CT to MH transformation was predicted for $FeSO_4F$/ $Mg_{0.5}FeSO_4F$ system. Cai et al. also predicted a similar CT to MH transformation in the $FeSO_4F$/ $LiFeSO_4F$ system[32] by first principles calculations.

Table 2 The average Bader charges around each nucleus in $FeSO_4F$ and $Mg_{0.5}FeSO_4F$.

Compound name	Average Bader charge(*e*)				
	Fe	S	O	F	Mg
$FeSO_4F$	+1.93	+3.91	-1.29	-0.66	
$Mg_{0.5}FeSO_4F$	+1.51	+3.86	-1.36	-0.77	+1.70

As Mg ions insert into cathode, electron would transfer from anode to the cathode material through the external circuit to maintain electrically neutral. To analyse the charge transfer mechanism accompanying with Mg ions intercalation quantitatively, the average Bader charge[33-35] around each nucleus in $FeSO_4F$ and $Mg_{0.5}FeSO_4F$ were calculated. As shown in Table 2, the Bader charges on Mg in $Mg_{0.5}FeSO_4F$ is +1.70 *e*, indicating the ionization of Mg. The charge of Fe are more than +3 e for $FeSO_4F$ and +2 e for $Mg_{0.5}FeSO_4F$, and the charge on O and F are also less than the classical oxidation state of O^{2-} and F^{1-}, suggesting the strong covalent interactions between Fe and O and F anions. After Mg ions intercalation, the Bader charge of each Fe atom changed from +1.93 *e* to +1.51 *e*, indicating that the insertion of one Mg reduced two FeO_4F_2 units instead of reducing only one FeO_4F_2 unit. The charge of O and F are changed only 0.07 e/atom and 0.11 e/atom from $FeSO_4F$ to $Mg_{0.5}FeSO_4F$, indicating that the charge transfer mechanism were mainly occurred on Fe atoms.

In order to investigate Mg ion conductivity in $Mg_{0.5-x}FeSO_4F$, the Cl-NEB method implemented in VASP was performed. As the previous study indicated that $Mg_{1-x}VPO_4F$ is a one dimensional Mg ion conductor[14], and the distance between adjacent Mg-vacancy along [100] and [001] directions of the super cell are longer than 7 Å, only Mg-vacancy diffusion barrier along [010] direction was calculated for $Mg_{0.5-x}FeSO_4F$. Fig.3 shows the diffusion paths for Mg-vacancy along [010] direction. There are two different sites for Mg-vacancy (labelled as A and B in Fig.3) in the unit cell of $Mg_{0.5}FeSO_4F$, and the Mg-vacancy was constructed by removing Mg ion from site A or B. Similar with Mg-vacancy diffusion path in $Mg_{1-x}VPO_4F$, the diffusion path for Mg-vacancy in $Mg_{0.5-x}FeSO_4F$ is a combination of two diagonal jumps: the jump from site A to site B labelled as L_1 and the jump from site B to site A labelled as L_2, then these diagonal jumps form continuous diffusion paths.

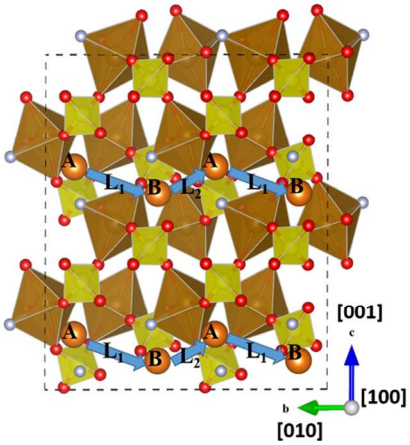

Fig.3 Mg-vacancy positions and its diffusion paths along [010] direction: the jump from site A to site B labelled as L1 and the jump from site B to site A labelled as L2.

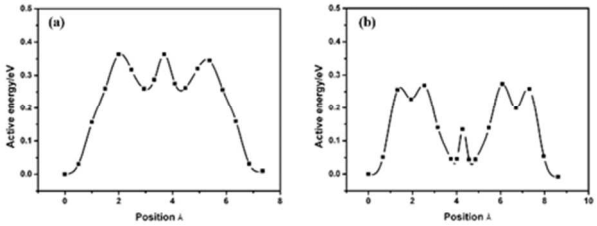

Fig.4 Minimum energy path for Mg-vacancy diffusion along [010] direction: (a) the jump from site A to site B and (b) the jump from site B to site A.

The energy barrier for Mg-vacancy diffusion along [010] direction is 0.36 eV, much lower than that of many bulk materials, such as V_2O_5 (1.40 eV)[15] and MoS_2 (2.61 eV)[12].

A rough diffusion coefficient can be estimate as[26]:

$$D = a^2 \nu e^{(-E_A/kT)}$$

Where a is the distant of a diffusion jump, ν is the attempt frequency and E_A is the activation energy, and kT is Boltzmann's constant times the temperature. In this calculation, a typical value of 10^{13} s^{-1} was used for ν, and the temperature was assumed to be 300*K*. An estimated diffusion coefficient using the highest activation energy is in the order of 10^{-9} cm^2/s, which is comparable to that of the calculated activation energy for Li^+ diffusion in $FeSO_4F$[26]. However, the available experimental diffusion coefficients for Li in tavorite-$FeSO_4F$/$LiFeSO_4F$ are several orders of magnitude lower than those predicted by theoretical calculations[30, 36, 37]. It should be noted that the experimental diffusion coefficient is not only related to the intrinsic ionic conductivity, but also related to the electrical conductivity and related to the defects in the diffusion channels[38]. It is worth noting that the diffusion coefficients were larger for

LiyFeSO4F in the Li-rich composition than in the Li-poor one, which is reasonably predicted by theoretical study. Indicating that theoretical calculation is helpful in qualitative analysis of ion diffusion mechanism. Therefore, the experimental diffusion coefficient for Mg-vacancy in $Mg_{0.5-x}FeSO_4F$ is expected to be in the same order of magnitude with that of Li-vacancy in $Li_{1-x}FeSO_4F$.

Conclusions

First principles calculations were performed to address the feasibility of tavorite-$FeSO_4F$ as new cathode materials for MIBs. The crystal structure, average OCV and electronic structures for $FeSO_4F$ and $Mg_{0.5}FeSO_4F$ were studied in detail. Phase separation of $Mg_{0.5}FeSO_4F/FeSO_4F$ is expected when Mg is extracted from $Mg_{0.5}FeSO_4F$ and a flat charge/discharge voltage curve at 2.52 V versus Mg/Mg^{2+} was predicted for $Mg_{0.5}FeSO_4F/FeSO_4F$. Tavorite-$FeSO_4F$ is a typical charge-transfer (CT) insulator and then transforms to a Mott-Hubbard (MH) insulator as Mg ion intercalation. The insertion of one Mg reduced two FeO_4F_2 units instead of reducing only one FeO_4F_2 unit, and the charge transfer mechanism were mainly occurred on Fe atoms. The activation energy for Mg-vacancy diffusion in $Mg_{0.5}FeSO_4F$ along [010] direction of the super cell is about 0.36 eV, which is comparable to that of Li^+ migration in $FeSO_4F$. In conclusion, the relatively high OCV and low intrinsic activation energy for Mg ion diffusion makes $Mg_{0.5}FeSO_4F$ to be a promising potential candidate for MIBs cathode materials.

Acknowledgements

The authors gratefully acknowledge the financial support by National Natural Science Foundation of China (grant numbers 51272179, 51102183, 51472182), Shanghai Committee of Science and Technology (11nm0501300, 13JC1408700), National high-tech R-D program of china (863 program) (grant no.2013AA031801), and Bayer Science & Education Foundation. The authors gratefully acknowledge Professor Wei Xu for providing computational resources. Some computations were also made possible thanks to Shanghai Supercomputer Center.

Notes and references

*Email: gao@tongji.edu.cn; wugm@tongji.edu.cn;
Shanghai Key Laboratory of Special Artificial Microstructure, Tongji University, Shanghai, P. R. China.

1. D. Aurbach, Z. Lu, A. Schechter, Y. Gofer, H. Gizbar, R. Turgeman, Y. Cohen, M. Moshkovich and E. Levi, *Nature*, 2000, **407**, 724-727.
2. Z. L. Tao, L. N. Xu, X. L. Gou, J. Chen and H. T. Yuan, *Chem. Commun.*, 2004, 2080-2081.
3. T. Ichitsubo, T. Adachi, S. Yagi and T. Doi, *J. Mater. Chem.*, 2011, **21**, 11764-11772.
4. A. Mitelman, M. D. Levi, E. Lancry, E. Levi and D. Aurbach, *Chem. Commun.*, 2007, 4212-4214.
5. Y. L. Liang, R. J. Feng, S. Q. Yang, H. Ma, J. Liang and J. Chen, *Adv. Mater.*, 2011, **23**, 640-+.
6. E. Levi, Y. Gofer and D. Aurbach, *Chem. Mater.*, 2010, **22**, 860-868.
7. E. Levi, M. D. Levi, O. Chasid and D. Aurbach, *J. Electroceram.*, 2009, **22**, 13-19.
8. S. Rasul, S. Suzuki, S. Yamaguchi and M. Miyayama, *Electrochim. Acta*, 2012, **82**, 243-249.
9. G. K. P. Dathar, D. Sheppard, K. J. Stevenson and G. Henkelman, *Chem. Mater.*, 2011, **23**, 4032-4037.
10. R. J. Xiao, H. Li and L. Q. Chen, *Chem. Mater.*, 2012, **24**, 4242-4251.
11. H. Moriwake, A. Kuwabara, C. A. J. Fisher, R. Huang, T. Hitosugi, Y. H. Ikuhara, H. Oki and Y. Ikuhara, *Adv. Mater.*, 2013, **25**, 618-622.
12. S. Q. Yang, D. X. Li, T. R. Zhang, Z. L. Tao and J. Chen, *Journal of Physical Chemistry C*, 2012, **116**, 1307-1312.
13. H. Lin, Y. W. Wen, C. X. Zhang, L. L. Zhang, Y. H. Huang, B. Shan and R. Chen, *Solid State Commun.*, 2012, **152**, 999-1003.
14. J. D. Wu, G. H. Gao, G. M. Wu, B. Liu, H. Y. Yang, X. W. Zhou and J. C. Wang, *Rsc Advances*, 2014, **4**, 15014-15017.
15. Z. G. Wang, Q. L. Su and H. Q. Deng, *PCCP*, 2013, **15**, 8705-8709.
16. J. Y. Huang, L. Zhong, C. M. Wang, J. P. Sullivan, W. Xu, L. Q. Zhang, S. X. Mao, N. S. Hudak, X. H. Liu, A. Subramanian, H. Y. Fan, L. A. Qi, A. Kushima and J. Li, *Science*, 2010, **330**, 1515-1520.
17. M. Nakayama, M. Kanekoa and M. Wakihara, *PCCP*, 2012, **14**, 13963-13970.
18. Z. J. Liu and X. J. Huang, *Solid State Ionics*, 2010, **181**, 1209-1213.
19. C. Ling, D. Banerjee, W. Song, M. J. Zhang and M. Matsui, *J. Mater. Chem.*, 2012, **22**, 13517-13523.
20. C. Ling and F. Mizuno, *Chem. Mater.*, 2013, **25**, 3062-3071.
21. S. C. Chung, P. Barpanda, S. Nishimura, Y. Yamada and A. Yamada, *PCCP*, 2012, **14**, 8678-8682.
22. S. Lee and S. S. Park, *Journal of Physical Chemistry C*, 2014, **118**, 12642-12648.
23. G. Kresse and J. Furthmuller, *Comp. Mater. Sci.*, 1996, **6**, 15-50.
24. J. P. Perdew, K. Burke and M. Ernzerhof, *Phys. Rev. Lett.*, 1996, **77**, 3865-3868.
25. S. L. Dudarev, G. A. Botton, S. Y. Savrasov, C. J. Humphreys and A. P. Sutton, *Phys. Rev. B: Condens. Matter*, 1998, **57**, 1505-1509.
26. T. Mueller, G. Hautier, A. Jain and G. Ceder, *Chem. Mater.*, 2011, **23**, 3854-3862.
27. G. Kresse and D. Joubert, *Phys. Rev. B: Condens. Matter*, 1999, **59**, 1758-1775.
28. P. E. Blochl, *Phys. Rev. B: Condens. Matter*, 1994, **50**, 17953-17979.
29. G. Henkelman, B. P. Uberuaga and H. Jonsson, *J. Chem. Phys.*, 2000, **113**, 9901-9904.
30. N. Recham, J. N. Chotard, L. Dupont, C. Delacourt, W. Walker, M. Armand and J. M. Tarascon, *Nature Materials*, 2010, **9**, 68-74.
31. Y. Koyama, I. Tanaka, M. Nagao and R. Kanno, *J. Power Sources*, 2009, **189**, 798-801.
32. Y. M. Cai, G. Chen, X. G. Xu, F. Du, Z. Li, X. Meng, C. Z. Wang and Y. J. Wei, *Journal of Physical Chemistry C*, 2011, **115**, 7032-7037.
33. G. Henkelman, A. Arnaldsson and H. Jonsson, *Comp. Mater. Sci.*, 2006, **36**, 354-360.
34. E. Sanville, S. D. Kenny, R. Smith and G. Henkelman, *J. Comput. Chem.*, 2007, **28**, 899-908.
35. W. Tang, E. Sanville and G. Henkelman, *Journal of Physics-Condensed Matter*, 2009, **21**.
36. C. Delacourt, M. Ati and J. M. Tarascon, *J. Electrochem. Soc.*, 2011, **158**, A741-A749.

37. S. L. Yang, L. P. Wang, R. G. Ma, Z. G. Lu, L. J. Xi, M. J. Hu, Y. C. Dong and C. Y. Chung, *J. Electrochem. Soc.*, 2013, **160**, A3072-A3076.
38. D. Morgan, A. Van der Ven and G. Ceder, *Electrochemical and Solid State Letters*, 2004, **7**, A30-A32.